Voprosy Onkologii = Problems in Oncology. 2025. Vol. 71, № 5
UDC 618.19-006
DOI 10.37469/0507-3758-2025-71-5-OF-2470

Seyede Nasrin Hosseinimotlagh, Abuzar Shakeri

Carbon Radiotherapy of Breast Tumor with Adding High-Z Metal Nanoparticles using GEANT4 Simulation Code

Department of Physics, Shi.C., Islamic Azad University, Shiraz, Iran

С.Н. Хоссейнимотлаг, А. Шакери

Лучевая терапия при раке молочной железы пучками углеродных ионов с применением наночастиц тяжелых металлов: моделирование в среде GEANT4

Кафедра физики, филиал в Ширазе, Исламский университет Азад, г. Шираз, Исламская Республика Иран

Radiotherapy (RT) is a vital approach in treating tumors, especially as a follow-up to surgical procedures in cancer therapy. In this article, we explored the advancements in treating breast tumors using carbon beams combined with varying concentrations of gold nanoparticles (GNPs). Our simulations, conducted with the GEANT4 code, indicate that as we increase the energy of the carbon beam and its distance from the starting point of the breast phantom, the absorbed dose tends to decrease. This is accompanied by a shift in the location of the Bragg peak (BP) to higher values of x as the incident carbon beam energy rises. Interestingly, we found that the lowest absorbed dose occurs in the absence of GNPs; however, as the injection rate of GNPs increases alongside the carbon beam irradiation, the absorbed dose rises compared to cases without GNP injection. This increase can be attributed to the presence of high-Z nanoparticles, like GNPs, which generate secondary electrons that enhance the dose deposited in both the tumor and its surrounding environment. Our findings suggest that for the studied phantom with the given geometry, a carbon beam energy range of 70 to 110 MeV/u is optimal, with the best results achieved at a Bragg's energy of 110 MeV/u.

Keywords: treatment; carbon; nanoparticles; absorbed dose; breast

For Citation: Seyede Nasrin Hosseinimotlagh, Abuzar Shakeri. Carbon radiotherapy of breast tumor with adding high-Z metal nanoparticles using GEANT4 simulation cod. *Voprosy Onkologii = Problems in Oncology.* 2025; 71(5): 1152-1161.-DOI: 10.37469/0507-3758-2025-71-5-OF-2470

Лучевая терапия (ЛТ) — основной метод лечения рака, особенно в качестве адъювантной терапии после хирургического вмешательства. В данной работе исследованы перспективы лечения рака молочной железы с использованием пучков углеродных ионов в комбинации с золотыми наночастицами в различных концентрациях. Проведенное нами моделирование в среде GEANT4 показало, что с увеличением энергии пучка углеродных ионов и расстояния от точки входа в фантом молочной железы поглощенная доза имеет тенденцию к снижению. Одновременно наблюдается смещение пика Брэгга в область больших значений глубины по мере роста энергии пучка. Примечательно, что минимальная поглощенная доза зарегистрирована в отсутствие золотых наночастиц; однако при совместном увеличении концентрации наночастиц и дозы облучения пучком углерода поглощенная доза возрастает по сравнению с контрольными условиями. Данный эффект объясняется присутствием наночастиц с высоким атомным номером, генерирующих вторичные электроны, которые усиливают дозу поглощенного излучения как в опухоли, так и в перитуморальной области. Результаты исследования свидетельствуют, что для использованной геометрии фантома оптимальный диапазон энергий пучка углеродных ионов составляет 70–110 МэВ/нуклон, с максимальной эффективностью при энергии Брэгга 110 МэВ/нуклон.

Ключевые слова: лучевая терапия; углеродные ионы; наночастицы; поглощенная доза; рак молочной железы

✉ Contact: Abuzar Shakeri, abuzar.shakeri6845@gmail.com

Introduction

For many years, various cancers, including breast cancer, have remained significant causes of death and challenges for society. At the early stages of breast cancer development, different imaging techniques and clinical tests can help with detection. Recently, efforts have concentrated on reducing breast cancer incidence through prevention, early detection, and treatment strategies [1]. The choice of treatment largely depends on the cancer type, as well as the tumor's size and progression. The primary treatment modalities currently employed include chemotherapy, surgery, hormone therapy, and radiation therapy [2–4]. Although patients with breast tumors generally have a better life expectan-

cy compared to those with other cancer types, existing treatments still struggle to completely eliminate these tumors and can also harm be surrounding healthy tissues [5–7].

Radiation therapy must be administered in a manner that accurately determines the dose delivered to the target area while minimizing harm to normal tissues, as this significantly improves treatment outcomes. The introduction of advanced high-energy accelerators in clinical settings during the 1950s marked a pivotal development in modern radiation therapy. The use of high linear energy transfer (LET) charged particles in radiation therapy has a storied history, beginning with carbon beams. Although heavier ion beams like neon, silicon, and argon have been explored in phase one clinical trials, only carbon ion beams are presently utilized in this form of treatment. The radiation characteristics of particle beams differ from those of conventional photons, leading to increased scientific interest in the radiobiological effects of high-LET therapies.

Among various ion beams, carbon ion radiotherapy (CIRT) has garnered significant attention due to its ability to deliver precise doses within the body while sparing surrounding tissues. This is largely made possible by the Bragg peaks that carbon beams produce, allowing effective target volume dosing. Given that protons are lighter than carbon ions, the radiobilogical effectiveness (RBE) of carbon ions is higher, particularly as penetration depth increases, reaching its peak at the end of the beam range [8–9]. This characteristic is particularly advantageous for therapy, as the RBE of carbon ion beams increases with greater penetration depth within tumor regions. One of the notable benefits of CIRT is the substantial reduction in side effects, as critical organs near the tumor are well protected from excessive radiation exposure.

Carbon ion therapy, including research at GSI at 1000 MeV/u, is a form of radiation treatment that uses carbon ions to target and destroy cancerous tumors. This approach is particularly effective due to the precise and well-localized dose deposition of carbon ions, which can be more effective than traditional radiation therapy for certain tumors and locations. The GSI facility, with its high beam intensity, enables FLASH irradiation for carbon ions, which is a very rapid delivery of radiation that can be beneficial in certain situations. Also in the Ref. [10] different beam energies of 400, 700, and 1,000 MeV/u were used.

Patients considered for carbon ion radiation therapy are typically evaluated based on four key clinical principles: 1) Local growth of cancerous tumors; 2) Tumors vary in their tendency to metastasize; 3) Some tumors display resistance to conventional treatments; and 4) The duration of treatment is often short, or side effects may be unacceptable with standard therapies [10]. In summary, the key factor in utilizing heavy ion particles in radiation therapy (RT) is the Bragg curve. Unlike photons, the trajectories of carbon ions are characterized by a Bragg peak (BP) at the end of their path [11]. By adjusting the kinetic energy of the incident ions, the BP can be precisely positioned at the desired depth within the cancerous tissue. Carbon ions and heavier ions exhibit two distinctive features: 1) Carbon ions have a similar RBE to photons at the same absorbed dose, while heavy ions possess a higher RBE; and 2) Heavy ions (unlike carbon ions) deliver a specific dose at the end of the BP, generating secondary fragmentation due to a complex radiation field [12].

Another promising approach to enhance RT involves the use of nanoparticles. Since 2004, notable results have emerged from employing high atomic number nanoparticles alongside radiation therapy. Experiments utilizing high-energy ions have also shown significant radiobiological efficiency improvements [13–18]. Gold nanoparticles (GNPs) have gained attention for their unique advantages: they are biocompatible, can be synthesized in various sizes, and their surfaces can be coated with diverse molecules to modulate surface charge and interactions with proteins [19–25]. The rationale behind using GNPs is that their combined application with radiation therapy stimulates the plasmons within these nanoparticles, leading to an increased yield of secondary electrons compared to pure water. Plasmons arise from nonlocalized electron excitations in materials.

The application of nanotechnology in the treatment of breast tumors has recently gained significant attention. Advances in this field have demonstrated that nanotechnology can improve breast cancer treatment outcomes [26–30]. It is evident that nanotechnology is crucial for the advancement of public health. Recent studies reveal that nanomaterials possess diverse physical, chemical, and biological properties that are intrinsically linked to their structural characteristics, making them valuable for developing innovative treatment systems for breast tumors [11–23]. A variety of nanomaterials have been synthesized, showcasing remarkable efficacy across multiple scientific disciplines, particularly in medicine. Researchers are currently exploring the potential of these nanomaterials in formulating anti-cancer medications, specifically targeting breast tumors. Their investigations focus on the effectiveness of nanomaterials in drug delivery systems, aiming to enhance therapeutic efficacy while minimizing toxicity to patients. However, despite the benefits associated with nanomaterials, challenges such as poor solubility and low reproducibility persist [14–16]. Additionally, the potential

toxicity of these materials necessitates careful consideration in their therapeutic applications. Another approach to improve radiation therapy involves the use of nanoparticles. In this context, the simultaneous administration of GNPs alongside carbon ion radiation is proposed for breast tumor treatment. GNPs are currently under extensive research for their potential in cancer therapy, demonstrating various clinical applications. This article examines feasibility of utilizing GNPs in breast cancer treatment to enhance diagnostic accuracy and radiation therapy. A quantitative assessment of dose enhancement in tumors enriched with GNPs, compared to adjacent healthy tissues, is conducted, highlighting their accessibility and compatibility with various chemical synthesis methods [17].

Research indicates that the injection of GNPs into tumor tissues can selectively enhance the efficacy of RT, resulting in a greater destruction of cancer cells. Notably, studies have demonstrated that the application of proton RT on tumors containing GNPs significantly improves the treatment's effectiveness against tumor cells. The potential of GNPs for both the treatment and diagnosis of tumors is expanding [28–30]. These biocompatible nanoparticles can be engineered to specific sizes and functionalized with various biological materials. It is important to highlight that the anticancer properties of GNPs, along with the safety and biological compatibility of gold, stem from their unique physical and chemical properties. The high atomic number of golds facilitates the absorption and enhancement of ionizing radiation.

Thus, introducing nanoparticles into tumors boosts the generation of free radicals, ultimately contributing to the destruction of cancer cells during treatment. Overall, research indicates that CIRT is more effective than proton beam therapy, allowing for treatment of a greater number of patients in the same timeframe. In the future, shortening treatment durations will reduce costs and enhance recovery efficiency for patients, making CIRT more accessible for both individuals and treatment facilities. The objective of this study is to investigate the effects of carbon therapy on breast tumors, both with and without the injection of GNPs into the cancerous tissue, utilizing the GEANT4 code.

Materials and Methods

Deposited Energy and Dose

A critical aspect of radiation therapy involves the estimation of the dose deposited within the tissue. This parameter is defined by the equation [21]: $D = dE\big/dm$, where dE represents the average energy deposited by the ionizing beam and dm denotes the mass element. In radiation therapy, water serves as the standard reference for tissue. The deposited dose in a target with a mass density ρ is expressed as follows [22]:

$$D[Gy] = 1{\cdot}6 \times 10^{-6} \times \frac{dE}{dx}\left[\frac{keV}{\mu m}\right] \times F[cm^{-2}] \times \frac{1}{\rho}\left[\frac{cm^3}{g}\right] \quad (1).$$

In this equation, dE/dx refers to the energy lost by a particle per unit length, commonly referred to as "stopping power" and F is flux. Recent studies indicate that for treatments involving a ^{12}C ion beam, the "RBE weighting dose" should be applied. Similar research is currently being conducted in the field of heavy ion therapy [23].

The process of halting energetic ions involves a review of fundamental equations pertinent to ion stopping within a dense adsorbent medium. The theoretical framework regarding the stopping power and range of ions in matter has been extensively examined in references [24–27]. The energy loss rate, denoted as dE/dx, is primarily influenced by inelastic scattering interactions with the target's electrons, a phenomenon that can be articulated through the Bethe-Bloch equation [28–30]. This equation incorporates terms for shell correction $(\frac{C}{Z_t})$ and effective density correction $(\frac{\delta}{2})$ [30]:

$$\frac{dE}{dx} = \frac{4\pi e^4 Z_t Z_P^2}{m_e v^2}\left[\ln\frac{2m_e v^2}{\langle I\rangle} - \ln(1-\beta^2) - \beta^2 - \frac{C}{Z_t} - \frac{\delta}{2}\right] \quad (2).$$

In this equation, β represents the ratio of velocity to the speed of light (v/c), while and signify the atomic numbers of the projectile and target, respectively. Additionally, e and refer to the charge and mass of the electron, respectively, and I, denotes the average ionization energy of the target atom or molecule. The energy dissipation is observed to increase as the particle energy decreases, due to the dependence on . At elevated velocities, atomic electrons are entirely stripped away, resulting in the projectile charge being equivalent to . Conversely, at lower velocities, the average charge diminishes due to the interplay between ionization and recombination, necessitating the substitution of in Equation (2) with , as described by the Barkas equation [30]:

$$Z_{eff} = Z_P\left[1 - exp\left(-125\beta Z_P^{-2/3}\right)\right] \quad (2).$$

Lower-energy projectiles play a significant role in energy dissipation through elastic collisions with nuclei, which predominantly governs the particle stopping mechanism towards the end of their trajectory. Given that the associated dose is minimal, it is often disregarded in beam therapy applications [31].

GNPs

GNPs studies utilize varying formulations in size, shape and surface moieties which have all

demonstrated noteworthy effects on sensitization. In proton therapy using GNPs, the distribution of the nanoparticles can be modeled as either homogeneous (uniformly dispersed) or heterogeneous (localized in specific areas). The density range of GNPs in this context usually refers to the concentration of nanoparticles within a given volume, often measured in mg/mL. The choice of model and density range significantly impacts dose enhancement and the potential for targeting tumor cells while sparing healthy tissue In the homogeneous model, nanoparticles are assumed to be evenly distributed throughout the target volume. This is a simplified model that can be useful for initial studies or when the exact location of nanoparticles is unknown. In contrast, the heterogeneous model assumes that nanoparticles are localized in specific areas, such as within the tumor cell nuclei or on the cell surface. This model more closely reflects the actual behavior of nanoparticles in vivo, where they tend to accumulate in certain areas due to factors like enhanced permeability and retention (EPR) effect. The density range of GNPs used in proton therapy typically ranges from a few mg/L to several tens of mg/L. The specific density range depends on the target volume, the intended therapeutic effect, and the specific synthesis and functionalization of the nanoparticles. It should be noted that in this article we have investigated the heterogeneous distribution of GNPs at the density range of 10 to 75mg/mL.

Modeling and simulation of GNPs distribution in tumor

Three kinds of spatial distributions can be considered for gold nanoparticles inside the tumor as below:

(i) Uniform distribution

(ii) Non-uniform distribution without any penetration margin

(iii) Non-uniform distribution with a margin for nanoparticles for penetration into healthy tissue.

Uniform distribution

This is the ideal case for distribution of nanoparticles. In this model, it was assumed that nanoparticles were uniformly distributed all over the tumor volume and there were no nanoparticles outside the tumor and therefore:

In this equation, a is the side of the cube and r is the distance of an arbitrary point from the tumor center. C is the concentration of GNPs. The calculations were carried out by Geant4, a general-purpose code for simulating the transport of particles through matter using Monte Carlo techniques. The version of Geant4.10.05.p01 was utilized and the simulations were performed for 10^8 histories for maximum accuracy and errors less than 5%. The tumor was modeled as a 1 × 1 × 1 cm cube in 2 cm depth (fig. 1). This volume was divided into 1 mm×1mm×1mm smaller cubes and the source was simulated as a point source. In each of such cubes, enough numbers of GNPs were defined according to the concentration of 10 ,25,50 and 75 mg/mL and size of 50 nm of GNPs. The average dose in the $1mm^3$ voxel was computed with and without the presence of GNPs. Then the absorbed dose was obtained.

This study employs the GEANT4 code for calculations. The GEANT4 methodology is applicable across all domains of medical physics and nuclear engineering, including radiation protection, radiotherapy, and nuclear medicine, and is noted for its high statistical accuracy. In this research, we present a hemispherical breast phantom with a radius of 8 cm, which encompasses adipose tissue and skin [44–46]. Within this phantom, a cube-shaped tumor measuring 2 cm is positioned 2 cm deep at the anterior aspect of the breast. Subsequently, a ^{12}C ion beam is directed towards the breast phantom from a distance of 15 cm, with an energy range of $70 \leq E\ (MeV/u) \leq 1000$, to evaluate the beam' s impact on the designated breast tumor. The phantom is then subjected to proton beam irradiation, incorporating GNPs into the cancerous tissue, and the absorbed dose results for both scenarios are compared.

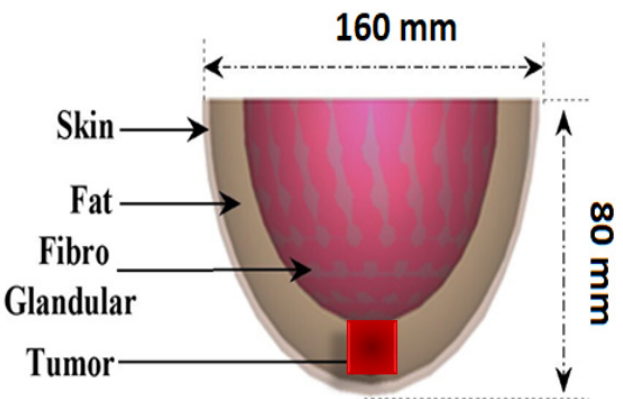

Fig. 1. Selected breast phantom

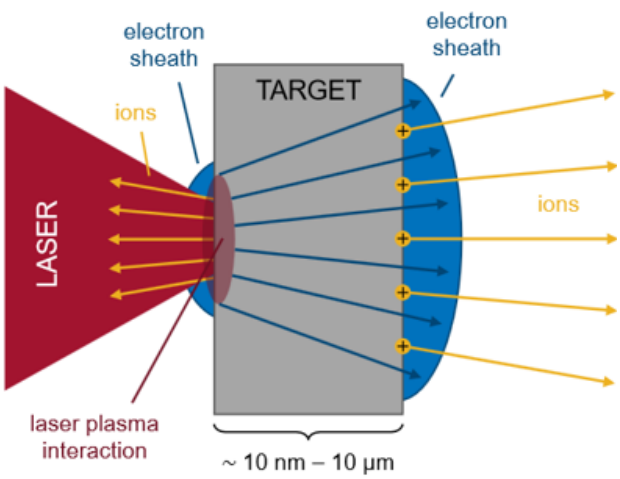

Fig. 2. Schematic of TNSA [31]

Target normal sheath acceleration (TNSA)

The acceleration of carbon and proton ions through the target normal sheath acceleration (TNSA) mechanism requires the presence of electrons to facilitate energy transfer from the laser to the ions. This ion acceleration occurs as a result of the interaction between an intense laser and a target, which generates high energy electrons. These electrons play a crucial role in the TNSA process, which will be elaborated upon further [31]. The TNSA mechanism was first introduced in 2001. As illustrated in fig. 2, this concept involves directing a high-intensity laser pulse onto a solid foil target, typically ranging in thickness from nanometers to micrometers.

The incident laser beam interacts solely with the surface of the foil, as the solid target foil possesses ultra-dense properties, leading to the formation of plasma following the laser radiation. The electrons within this plasma are energized by the laser pulse, acquiring kinetic energy and subsequently departing from the rear area where the interaction occurred. A portion of these energized electrons traverses the target and exits from the back. The electric fields generated ionize the atoms located behind the target, resulting in a charge separation field and the establishment of an electron shell with a thickness that corresponds to the Debye length: $\lambda_D = \sqrt{T_e / 4\pi n_e e^2}$, where T_e, n_e, and e represent electron temperature, electron density, and electron charge, respectively. A continuous accumulation of electrons occurs due to the charge separation field surrounding the target, while the sheath is safeguarded by the influx of new electrons generated from laser-plasma interactions at the front surface of the heated target. Consequently, this electron sheath produces a robust quasi-static electric field that influences the ions on the rear surface of the target, resulting in their acceleration predominantly in a direction normal to the target. As illustrated in Fig. 2, an electron shell emerges at the front side of the target, leading to the acceleration of lower energy ion particles in a direction opposite to that of the ions in the rear region of the target. The mechanism of TNSA fundamentally differs from the functioning of traditional particle accelerators. Notably, the ions that are accelerated exhibit a broad spectrum of kinetic energy.

Results

In this study, the effect of uniform distribution of GNPs in the tumor, with 50 nm nanoparticle size, the effect of energy on the tumor dose enhancement into healthy tissues around the tumor were taken into consideration. In human tissues, the total stopping power of charged particles, like protons or electrons, is the sum of electronic and

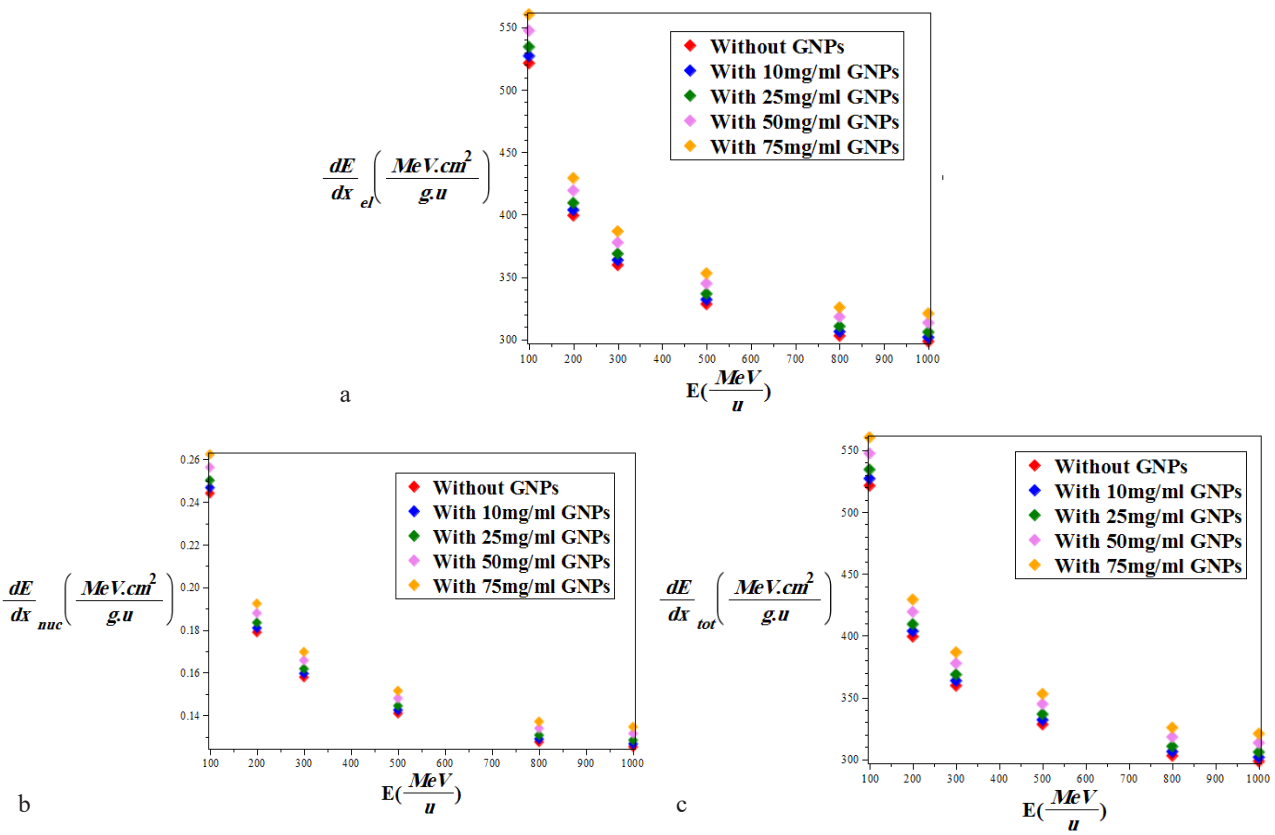

Fig. 3: (a) electron, (b) nuclear and (c) total mass stopping power of ^{12}C ion with and without injecting of GNPs for different concentrations in breast phantom

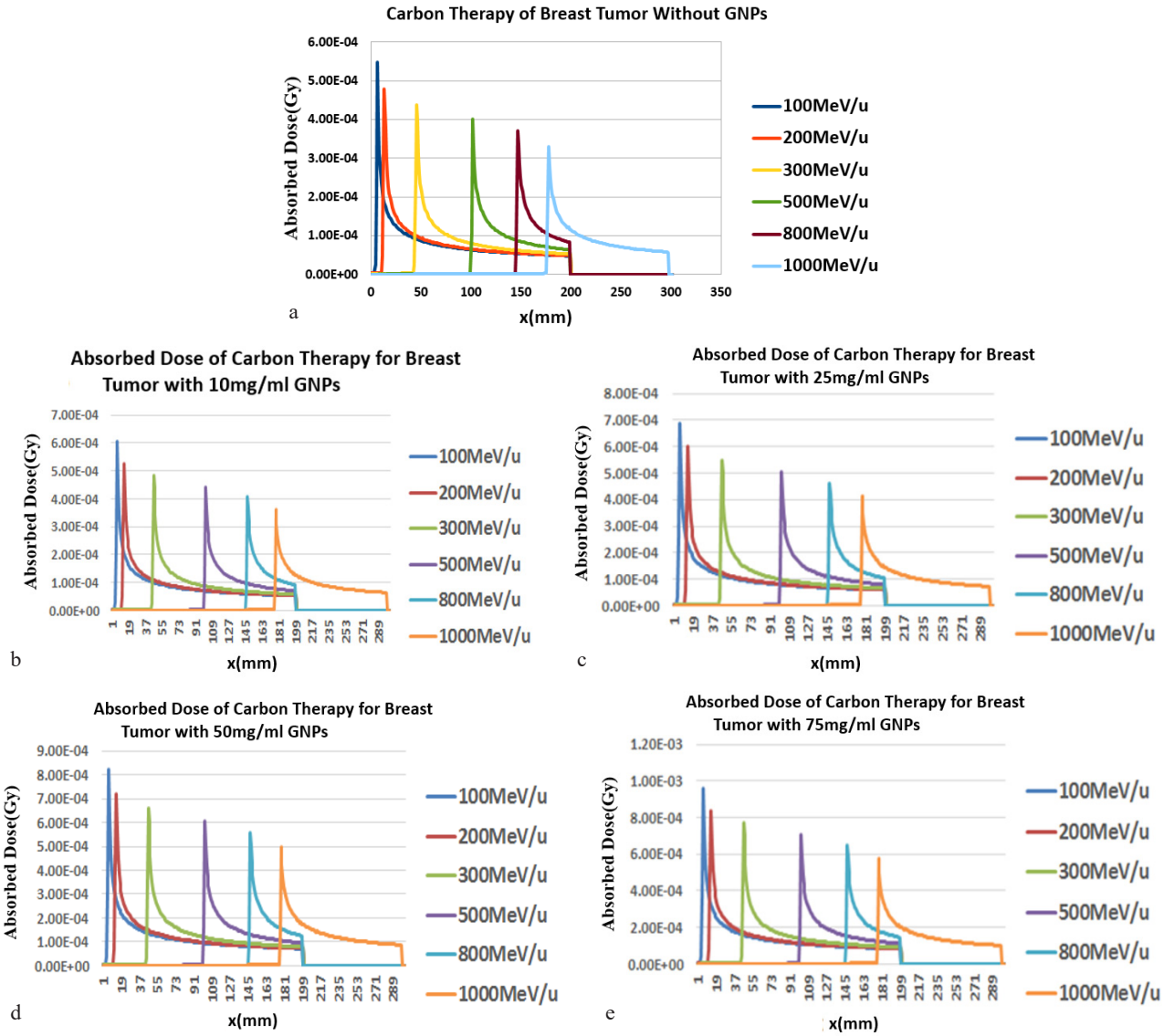

Fig. 4. Simulated absorbed dose with GEANT4 code in the breast phantom using different injection rate of GNPs versus penetration depth for different carbon energies (note: we used as spherical GNPs with diameter= 50 nm)

nuclear stopping power. Electronic stopping power, which is the primary component at higher energies, arises from inelastic collisions with the target's electrons, leading to ionization and excitation. Nuclear stopping power, on the other hand, results from elastic collisions with the target's nuclei, and it is significant only at low energies.

This section presents a classification of the findings related to stopping power and absorbed dose, derived from the GEANT4 simulations [17]. In fig. 3 and 4, the results illustrating the variations in the determination of electron, nuclear, and total mass stopping power, as well as the absorbed dose, are presented in relation to carbon ion energy within the energy range of $70 \leq E$ (MeV/u) ≤ 1000. This analysis was conducted in breast tissue using GEANT4 simulation for two scenarios: (i) with the injection of GNPs and (ii) without the injection of GNPs in the proposed phantom.

The calculations were carried out by Geant4, a general-purpose code for simulating the transport of particles through matter using Monte Carlo techniques. The version of Geant4.10.05.p01 was utilized and the simulations were performed for 10^8 histories for maximum accuracy and errors less than 5 %.

The tumor, measuring 2 cm in depth and 2 cm in width, indicates that the optimal energy of BP, in the absence of GNPs injection, is 110 MeV/u, as illustrated in Fig. 5(a), 5(b), 5(c), 5(d) and 5(e).

According to different studies, when the ions passing through the matter will suffer the multiple scattering and lose their kinetic energies partially. The mechanism of ion energy loss is strongly the function of medium's density. Hence, the high-Z materials like gold not only will cause the highest rate of interactions with the incident ions and releas-

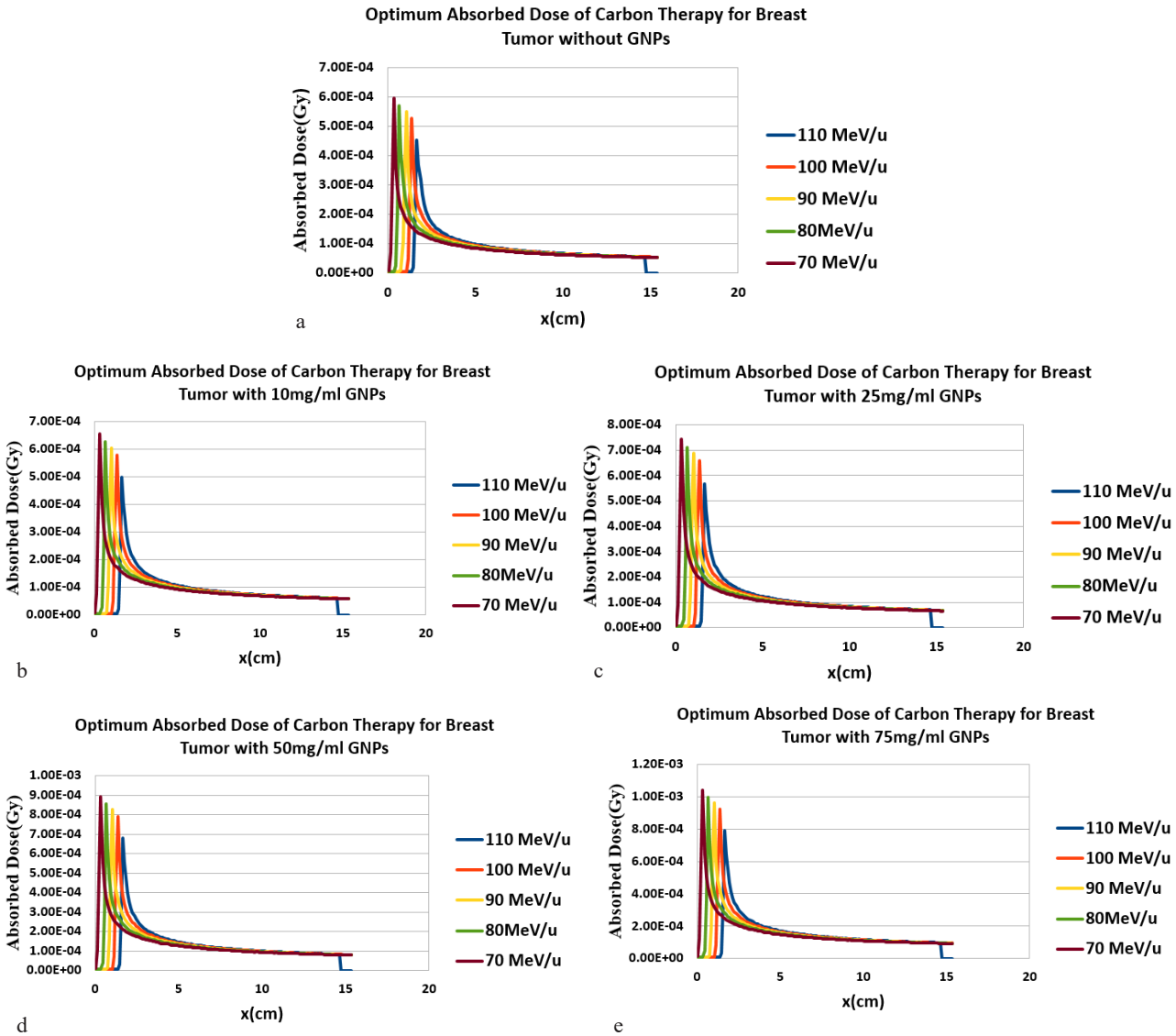

Fig. 5. Simulated absorbed dose with GEANT4 code in the optimal energy range of BP of breast phantom using different injection rate of GNPs versus penetration depth for different carbon energies (note: we used as spherical GNPs with diameter = 50 nm)

ing a large number of secondary electrons through the ionization of gold atoms also cause that, ions lose their energies when traversing the nanoparticles. Also, the biological effectiveness of ions as the function of LET is strongly depending on their kinetic energies [26]. Hence, when ions lose their kinetic after leaving the GNP, it is expected that, their biological impact increase when their kinetic energies have reduced. In this work, we showed that, the ion after exiting the GNPs will perform the greater effects than of the released electrons. In carbon therapy, the secondary electron spectrum, produced by the interaction of carbon ions with target material, is a key factor in the therapy's effectiveness. These electrons play a significant role in the energy deposition and subsequent biological effects. The peak of the secondary electron energy distribution is generally found between 12 and 15 keV (fig. 6).

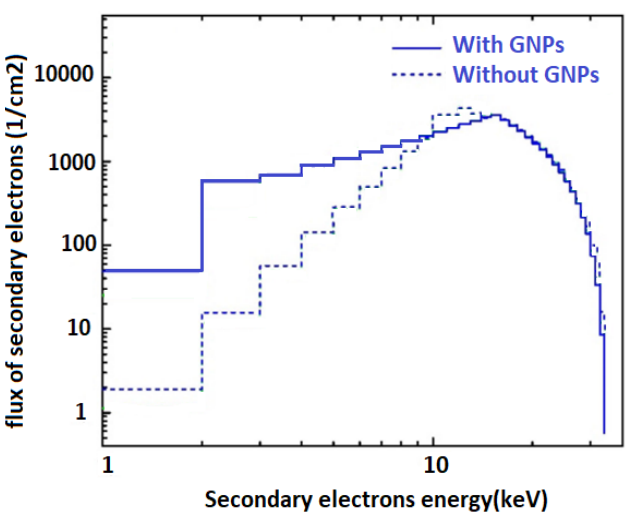

Fig. 6. The flux of the secondary electrons per incident carbon beam for with (75mg/mL) and without GNPs injection

Discussion

The analysis of fig. 3(a), 3(b), and 3(c) reveals that as the energy of the ^{12}C ion increases, the results of the mass stopping power exhibit a density effect and an increase in the production of secondary electrons. This indicates that the interactions between electrons and charged particles are influenced by atomic interference. As the frequency of collisions between atoms and electrons within the electric field of polarized charged particles diminishes, the MSP correspondingly decreases. Furthermore, relativistic effects amplify the significance of these collisions, leading to an increase in this effect at higher energy levels, a phenomenon referred to as the density effect. Typically, the mass stopping power ratio between two distinct materials—one solid and the other either liquid or gaseous—exhibits a gradual variation with respect to particle energy. This ratio diverges due to the reduction of solid mass stopping power as the particle energy approaches relativistic thresholds. Fig. 4(a), 4(b), 4(c),4(d) and 4(e) illustrate that as both distance and energy increase from the initial point within the breast phantom, the dose within the breast phantoms diminishes, and the position of the breast phantom shifts towards larger x-values with the escalation of ^{12}C ion energy. Our simulations indicate that the minimum absorbed dose occurs in the absence of GNPs, while an increase in the injection rate of GNPs at 10, 25, 50, and 75 mg/ml results in a higher absorbed dose compared to the scenario without GNPs. This outcome can be attributed to the presence of high atomic number nanoparticles, such as GNPs, which enhance the deposited dose in the tumor or surrounding tissue through the increased generation of secondary electrons. Notice that using nanoparticles with a higher atomic number can lead to greater damage to surrounding healthy tissues. This is because high-Z nanoparticles increase the number of secondary electrons generated during irradiation, which can deposit more energy in the surrounding medium and thus increase the overall radiation dose and damage to the tissue.

The corresponding absorbed dose is calculated to be per 5 million carbon atoms in the beam. In scenarios where GNPs are injected at concentrations of 10, 25, 50, and 75 mg/ml, the optimal energy of BP remains at 110 MeV/u. However, the absorbed dose at this optimal energy increases with higher concentrations of gold, yielding absorbed dose values of , ,and , respectively, for the specified concentrations. Based on the current study with GEANT4 simulation code, it is shown that in a certain concentration, GNPs with higher dimensions contribute more dose to the tumor volume; while in a uniform distribution of GNP causes a remarkable increase in the absorbed dose.

This work gives an opportunity to calculate the energy spectra of secondary electrons produced by energetic ions incident on breast tissue. In order to report these electron energy distributions with the best possible accuracy for each ion energy range, we consider EM_Livermore model in this simulation [fig. 6]. Fig. 6 shows that injection of GNPs simultaneously with carbon beam irradiation increases the flux of secondary electrons produced in breast tissue. The error caused by induced secondary electrons is significant, and can vary depending on the material, the energy of the incident beam, and the experimental setup. While the exact percentage of error is not a single, universal value, studies suggest it can range from 5-10 % to potentially 20 % or more, depending on the specific code.

Conclusion

High-energy ^{12}C ion beams present significant advantages in the treatment of deep localized tumors when compared to traditional MV photon therapy. The biological effects of ^{12}C ions in the Bragg Peak (BP) region are particularly beneficial, making them a promising option for addressing radio-resistant tumors located near sensitive organs. This study introduces a flexible model capable of simulating the concentrations of GNPs utilized in treatment, which can be established with a relatively low-cost setup. Unlike other models that focus on a single nanoparticle, this model effectively demonstrates large-scale effects and analyzes variations in BPs for different nanoparticle concentrations. In this research, the GEANT4 simulation code was employed for tumor therapy involving a 2 cm thick tumor located 2 cm deep from the surface of the selected phantom. Our findings indicate that for the proposed phantom with the specified geometry, a carbon beam energy range of 70 to 110 MeV/u is optimal, with the ideal Bragg peak energy being 110 MeV/u. The plotted Fig.s illustrate that as carbon energy increases; the penetration power of the particles also rises. Consequently, with greater particle penetration depth, the frequency of inelastic collisions with the nuclei of the target material increases, leading to a reduction in BP height and transverse broadening. This study highlights those advancements in simulations for carbon therapy reveal that various factors, such as total mean square pressure, absorbed dose, the concentration of injected GNPs, the type and thickness of the target material, and the energy of carbon radiation, are interrelated. GNPs due to their high atomic number (Z) provide remarkable effects lead to enhancement of absorbed radiation dose in a tumor. This is due to a wide range of produced secondary electrons inside and in the vicinity of the tumor. The observations and results confirmed that GNPs can increase the

dose of the tumor during radiotherapy. Furthermore, the injection and increased concentration of GNPs into breast tissue result in an enhanced absorbed dose, attributed to the effects of density and the amplification of secondary electrons.

Authors' contributions

All authors made a substantial contribution to the conception of the work, acquisition, analysis, interpretation of data for the work, drafting and revising the work, final approval of the version to be published.

REFERENCES

1. Sulaiman N.S., Demizu Y., Koto M., et al. Multicenter study of carbon-ion radiation therapy for adenoid cystic carcinoma of the head and neck: subanalysis of the Japan carbon-ion radiation oncology study group (J-CROS) study (1402 HN). *Int J Radiat Oncol Biol Phys*. 2018; 100: 639–46.-DOI: https://doi.org/10.1016/j.ijrobp.2017.11.010.
2. Koto M., Demizu Y., Saitoh J.I., et al. Multicenter study of carbon-ion radiation therapy for mucosal melanoma of the head and neck: subanalysis of the Japan carbon-ion radiation oncology study group (J-CROS) study (1402 HN). *Int J Radiat Oncol Biol Phys*. 2017; 97: 1054–60.-DOI: https://doi.org/10.1016/j.ijrobp.2016.12.028.
3. Bhattacharyya T., Koto M., Ikawa H., et al. First prospective feasibility study of carbon-ion radiotherapy using compact superconducting rotating gantry. *Br J Radiol*. 2019; 92: 20190370.-DOI: https://doi.org/10.1259/bjr.20190370.
4. Sokol O., Durante M. Carbon ions for hypoxic tumors: are we making the most of them? *Cancers* (Basel) 15:4494.-DOI: https://doi.org/10.3390/cancers15184494.
5. Hagiwara Y., Bhattacharyya T., Matsufuji N., et al. Influence of dose-averaged linear energy transfer on tumour control after carbon-ion radiation therapy for pancreatic cancer. *Clin Transl Radiat Oncol*. 2020; 21: 19–24.-DOI: https://doi.org/10.1016/j.ctro.2019.11.002.
6. Matsumoto S., Lee S.H., Imai R., et al. Unresectable chondrosarcomas treated with carbon ion radiotherapy: relationship between dose-averaged linear energy transfer and local recurrence. *Anticancer Res*. 2020; 40: 6429–35.-DOI: https://doi.org/10.21873/anticanres.14664.
7. Morelli L., Parrella G., Molinelli S., et al. A dosiomics analysis based on linear energy transfer and biological dose maps to predict local recurrence in sacral chordomas after carbon-ion radiotherapy. *Cancers* (Basel). 2022; 15: 33.-DOI: https://doi.org/10.3390/cancers15010033.
8. Okonogi N., Matsumoto S., Fukahori M., et al. Dose-averaged linear energy transfer per se does not correlate with late rectal complications in carbon-ion radiotherapy. *Radiother Oncol*. 2020; 153: 272–8.-DOI: https://doi.org/10.1016/j.radonc.2020.08.029.
9. Mori Y., Okonogi N., Matsumoto S., et al. Effects of dose and dose-averaged linear energy transfer on pelvic insufficiency fractures after carbon-ion radiotherapy for uterine carcinoma. *Radiother Oncol*. 2022; 177: 33–9.-DOI: https://doi.org/10.1016/j.radonc.2022.10.008.
10. Guardiola C., Prezado Y.. High-energy charged particles for spatially fractionated radiation therapy. *Front Phys*. 2020; 8: 299.-DOI: https://doi.org/10.3389/fphy.2020.00299.
11. Kohno R., Koto M., Ikawa H., et al. High–linear energy transfer irradiation in clinical carbon-ion beam with the linear energy transfer painting technique for patients with head and neck cancer. *Adv Radiat Oncol*. 2023.-DOI: https://doi.org/10.1016/j.adro.2023.101317.
12. Das S., Dey M.K., Devireddy R., Gartia M.R. Biomarkers in cancer detection, diagnosis, and prognosis. *Sensors*. 2024; 24(1): 37.-DOI: https://doi.org/10.3390/s24010037.
13. Pillai G. Nanotechnology toward treating cancer. Applications of targeted nano drugs and delivery systems. 2019; 221–56.-DOI: https://doi.org/10.1016/B978-0-12-814029-1.00009-0.
14. Eisenhauer E.A., Therasse P., Bogaerts J., et al. New response evaluation criteria in solid tumours: revised RECIST guideline (version 1.1). *Eur J Cancer version*. 2009; 228–47; 1: 45.-DOI: https://doi.org/10.1016/j.ejca.2008.10.026.
15. Koto M., Hasegawa A., Takagi R., et al. Feasibility of carbon ion radiotherapy for locally advanced sinonasal adenocarcinoma. *Radiother Oncol*. 2014; 113: 60–5.-DOI: https://doi.org/10.1016/j.radonc.2014.09.009.
16. Inaniwa T., Kanematsu N., Matsufuji N., et al. Reformulation of a clinical-dose system for carbon-ion radiotherapy treatment planning at the National Institute of Radiological Sciences. *Japan Phys Med Biol*. 2015; 60: 3271–86.-DOI: https://doi.org/10.1088/0031-9155/60/8/3271.
17. Rosenfeld A.B. Novel detectors for silicon based microdosimetry, their concepts and applications. *Nucl Instrum Methods Phys Res A*. 2016; 809: 156–70.-DOI: https://doi.org/10.1016/j.nima.2015.08.059.
18. Lee S.H., Mizushima K., Kohno R., et al. Estimating the biological effects of helium, carbon, oxygen, and neon ion beams using 3d silicon microdosimeters. *Phys Med Biol*. 2021; 66: 045017.-DOI: https://doi.org/10.1088/1361-6560/abd66f.
19. Mizoe J.E., Hasegawa A., Jingu K., et al. Results of carbon ion radiotherapy for head and neck cancer. *Radiother Oncol*.-DOI: 2012; 103: 32–7. https://doi.org/10.1016/j.radonc.2011.12.013.
20. Kopp B., Mein S., Dokic I., et al. Development and validation of single field multi-ion particle therapy treatments. *Int J Radiat OncolBiol Phys*. 2020; 106: 194–205.-DOI: https://doi.org/10.1016/j.ijrobp.2019.10.008.
21. Ebner D.K., Frank S.J., Inaniwa T., et al. The emerging potential of multi-ion radiotherapy. *Front Oncol.* 2021; 11: 624786.-DOI: https://doi.org/10.3389/fonc.2021.624786.
22. Inaniwa T., Suzuki M., Hyun Lee S.H., et al. Experimental validation of stochastic microdosimetric kinetic model for multi-ion therapy treatment planning with helium-, carbon-, oxygen-, and neon-ion beams. *Phys Med Biol*. 2020; 65: 045005.-DOI: https://doi.org/10.1088/1361-6560/ab6eba.
23. Pompos A., Foote R.L., Koong A.C., et al. National effort to re-establish heavy ion cancer therapy in the United States. *Front Oncol*. 2022; 12: 880712.-DOI: https://doi.org/10.3389/fonc.2022.880712.
24. Bag N., Bardhan S., Roy S., et al. Nanoparticle-mediated stimulus-responsive antibacterial therapy. Biomater Sci. 2023; 11(6): 1994–2019.-DOI: https://doi.org/10.1039/d2bm01941h.
25. Baghirov H. Receptor–mediated transcytosis of macromolecules across the blood–brain barrier. Expert Opin Drug Deliv. 2023; 20(12): 1699–711.-DOI: https://doi.org/10.1080/17425247.2023.2255138.
26. Ezhilarasan D., Shree Harini K. Nanodrug delivery: Strategies to circumvent nanoparticle trafficking by Kupffer cells in

the liver. J Drug Deliv Sci Technol. 2023; 86: 104731.-DOI: https://doi.org/10.1016/j.jddst.2023.104731
27. Campos B., Olsen L.R., Urup T., Poulsen H.S. A comprehensive profile of recurrent glioblastoma. *Oncogene*. 2016; 35(45): 5819–25.-DOI: https://doi.org/10.1038/onc.2016.85.
28. Chang C., Wang C., Zhang C., et al. Albumin-encapsulated platinum nanoparticles for targeted photothermal treatment of glioma. J Biomed Nanotechnol. 2019; 15(8): 1744–53.-DOI: https://doi.org/10.1166/jbn.2019.2803.
29. Chen X., Momin A., Wanggou S., et al. Mechanosensitive brain tumor cells construct blood-tumor barrier to mask chemosensitivity. *Neuron*. 2023; 111(1): 30-48.e14.-DOI: https://doi.org/10.1016/j.neuron.2022.10.007.
30. Chester C., Sanmamed M.F., Wang J., Melero I. Immunotherapy targeting 4-1BB: mechanistic rationale, clinical results, and future strategies. *Blood.* 2018 Jan 4; 131(1): 49–57.-DOI: https://doi.org/10.1182/blood-2017-06-741041.
31. Reddy S., Tatiparti K., Sau S., Iyer A.K. Recent advances in nano delivery systems for blood-brain barrier (BBB) penetration and targeting of brain tumors. *Drug Discovery Today*. 2021; 26(8): 1944–52.-DOI: https://doi.org/10.1016/j.drudis.2021.04.008.

Received / 14.08.2025
Reviewed / 24.10.2025
Accepted for publication / 29.10.2025

Author Information / ORCID

Seyede Nasrin Hosseinimotlagh / ORCID ID: https://orcid.org/0000-0001-5381-2449
Abuzar Shakeri / ORCID ID: https://orcid.org/0009-0007-8075-6711.